# Phantom Design and Verification Enabling Effective Antennas for Bird Tracking Technology

Bryan A. Sandoval, *Member, IEEE*, Eli S. Bridge, Caleb F. Fulton, *Senior Member, IEEE*, and Jessica E. Ruyle, *Senior Member, IEEE*

***Abstract*—Advances in miniaturized radio tracking technology are helping to revolutionize the field of wildlife biology, especially with respect to studies of small birds. However, development of antennas for animal tracking applications often fails to formally account for the effects of the animal's body on signal transmission. This letter describes an electromagnetic phantom that accurately represents a small bird. The phantom is validated with empirical measurements and can be easily scaled to represent larger or smaller bird species.**

***Index Terms*—Bird tracking, dark-eyed junco (*Junco hyemalis*), phantom.**

## I. Introduction

ORNITHOLOGISTS have been studying bird movement patterns for decades, and miniaturized tracking technologies have led to major advances in understanding of phenomena like migration and habitat use [1]–[6]. Although development of tracking technologies for birds has been ongoing for decades, development of effective antennas for radio-telemetry devices has involved considerable guesswork with regard to how the body tissues of a bird affect signal transmission. To date, attempts to model or simulate a bird body involved assuming the effect of the animal's body is negligible or equivalent to a volume of saline. For example, in [7], a simple bird model was designed with two ellipsoid shapes with the electrical properties of saline ($\epsilon_r = 75$ and $\sigma = 2$ S/m) to represent the head and the torso of a bird. Although this model was a critical first step, there was no formal attempt to justify equating the birds tissues to saline or to otherwise validate the accuracy of the model.

This letter describes a more realistic bird phantom designed in high frequency structure simulator (HFSS) [8] that accurately represents the material properties that have been empirically measured with salvaged carcasses of dark-eyed juncos (*Junco hyemalis*). Dark-eyed juncos are a common species that has been the subject of numerous tracking studies [9]. Additionally, dark eyed juncos are a representative size and anatomy of a small bird for which ongoing development of tracking technology is needed. This letter will begin with a discussion of the bird phantom. The properties of the phantom described in the initial section will be justified through antenna measurements discussed in Section III. Finally, a comparison of the simulated and measured results with the phantom and bird carcasses will be discussed in Section IV and will be followed with conclusions.

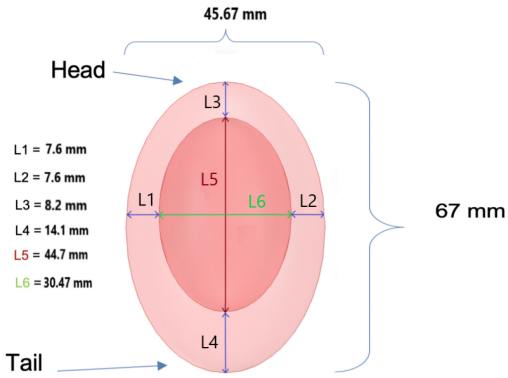


Fig. 1. Bird phantom with nested ellipsoids to represent both feathers and wet tissue.

## II. Bird Phantom

The phantom is configured as an ellipsoid within an ellipsoid, where the outer volume represents the feathers and the inner volume represents wet tissue as shown in Fig. 1. This arrangement of volumetric structures accurately simulates the dominant dielectric and geometrical features, yet is simple enough to allow for straightforward scaling to generate representations for a variety of bird species. The phantom structure was initially conceived as a more complex model with additional ellipsoids that represented the interconnected air sacs found in all birds. However, the virtual air sacs did not contribute to the accuracy of the model with regard to its electric properties. Hence, a simplified model, without air sacs is presented here. This letter represents the first step toward a comprehensive phantom library to propel antenna designs for bird tracking technology.

The properties of the bird phantom are presented in this section. The justification for these properties will be given in the next two sections. An outer volume with a relative permittivity

Manuscript received 9 March 2022; revised 4 April 2022; accepted 6 April 2022. Date of publication 27 May 2022; date of current version 4 August 2022. *(Corresponding author: Jessica E. Ruyle.)*

Bryan A. Sandoval, Caleb F. Fulton, and Jessica E. Ruyle are with the School of Electrical Engineering and the Advanced Radar Research Center (ARRC), University of Oklahoma, Norman, OK 73019 USA (e-mail: byan.sandoval@ou.edu; fulton@ou.edu; ruyle@ou.edu).

Eli S. Bridge is with the Oklahoma Biological Survey, University of Oklahoma, Norman, OK 73019 USA (e-mail: ebridge@ou.edu).

Digital Object Identifier 10.1109/LAWP.2022.3178292

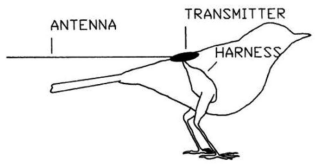


Fig. 2. Illustration of a leg-loop harness for bird trackers from [12].

of 1.2 and a conductivity value of 0 S/m and an inner volume with a relative permittivity of 1.2 and a conductivity value of 3 S/m provided the best match between simulated and measured results. It is important to note that the inner volume is slightly offset and not centered. This was done to represent the abundance of feathers at the tail end of the bird carcass. The salvaged bird carcass was measured to have 67 mm in length and 45.67 mm in width, which was set as the outer volume dimensions. In order to compensate for the average width and length of feather around the torso, an inner torso volume was set to an average length of 44.7 mm and a width of 30.47 mm, while the space between the two volumes is the average dimensions of feathers around the bird carcass. This is annotated in Fig. 1.

## III. Antenna Design and Measurements

A monopole antenna was chosen to verify the phantom due to its simplicity and field similarity to traditionally used antennas for bird tagging. The monopole was chosen over a dipole to eliminate the need for a balun as the balun would add significant complexity to the measurement. A ribbon monopole antenna was designed, simulated, and fabricated at the operating frequency of 2.85 GHz. The frequency of 2.85 GHz was chosen to enable tag design in the weather radar frequency band—allowing bird tracking with already constructed and maintained infrastructure. While 2.85 GHz is above some frequencies used for bird tracking [10], [11], the higher frequency used here should simply provide increased sensitivity and the phantom presented here should maintain a reasonable level of accuracy at lower frequencies.

The ribbon (length 21.4 mm) was designed as 1/2 oz copper trace material backed with 30 mil Rogers 5880. The ground plane was a square with side length of twice the wavelength (21.43 cm) and constructed using 1/2 oz copper 60 mil Rogers 4350. The monopole was designed with an SMA connector feeding the antenna through a hole in the ground plane as is typical. The RMS error between simulated and measured results for the monopole of both return loss and impedance was within of 5% across the entire frequency band while RMS error between simulated and measured realized gain across all measured cut-planes was within 6%. Therefore, the constructed monopole can be used to find appropriate material properties for the phantom by comparing simulated and measured values.

The fabricated monopole was measured both in free space and mounted in direct contact with two different bird carcasses. The dark-eyed juncos (*Junco hyemalis*) used for measurements were salvaged carcasses that were frozen for preservation and thawed

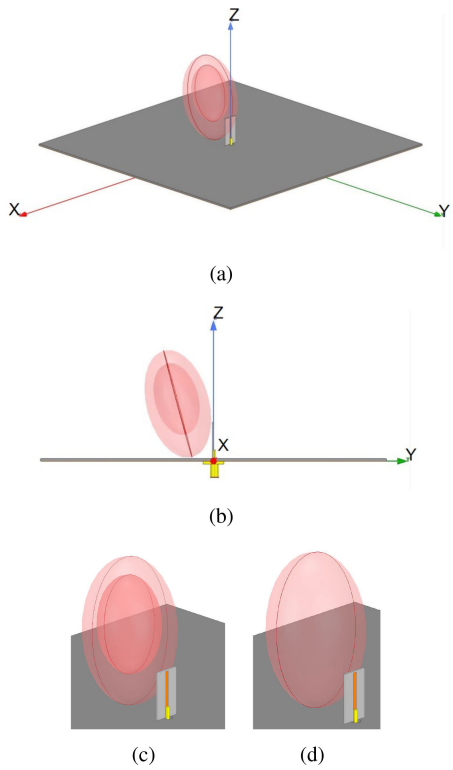


Fig. 3. Simulated ribbon monopole with bird phantom with depictions of (a) dimetric view, (b) side view, (c) dimetric view closer to the antenna, and (d) saline phantom used for comparison in this paper with only one solid ellipsoid and material properties as suggested in [7].

before any measurements were taken. Tracking devices for small birds are typically mounted on the lower back using a leg-loop harness as shown in Fig. 2. A position for the monopole that most closely emulated this typical antenna mount was chosen. In Fig. 3, the simulated ribbon monopole antenna is shown with the bird phantom. For testing, the ribbon monopole was vertically oriented and a styrofoam mount was used to position the lower back of the bird against the antenna with the copper traces facing outward and away from the bird (see Fig. 3). Two different dark-eyed juncos (*Junco hyemalis*) were used for the bird measurements—labeled as Bird 1 and Bird 2 for comparison. Bird 1 had been dead and frozen for about a year and a half, while Bird 2 had a more recent death of about 2 weeks prior to measurements. In physical appearance, Bird 1 was slightly bigger (about 10–15 mm in additional length) than Bird 2.

Fig. 4 shows the magnitude of the insertion loss ($|S_{11}|$) and input impedance for the fabricated monopole in free space and mounted next to Birds 1 and 2. The figure shows that Birds 1 and 2 slightly shifted the resonance and in the case of Bird 2 provided a higher insertion loss dip. Both of these figures illustrate that the birds did not have a significant impact on impedance behavior of the ribbon monopole.

Fig. 5 shows the copolarized radiation patterns for the fabricated monopole in free space and mounted next to Birds 1 and 2. It can be seen in this figure that the birds have more impact on

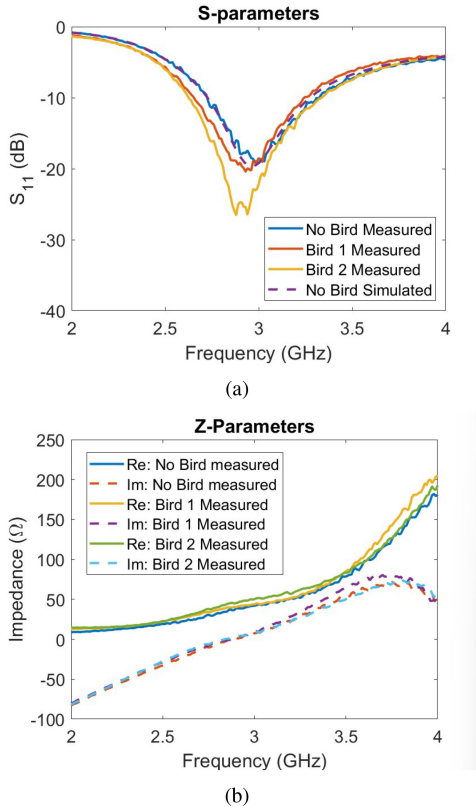


Fig. 4. Measurements of monopole placed next to birds compared to free space measurements and simulations with (a) showing magnitude of insertion loss ($|S_{11}|$) in dB and (b) showing input impedance ($Z_{11}$).

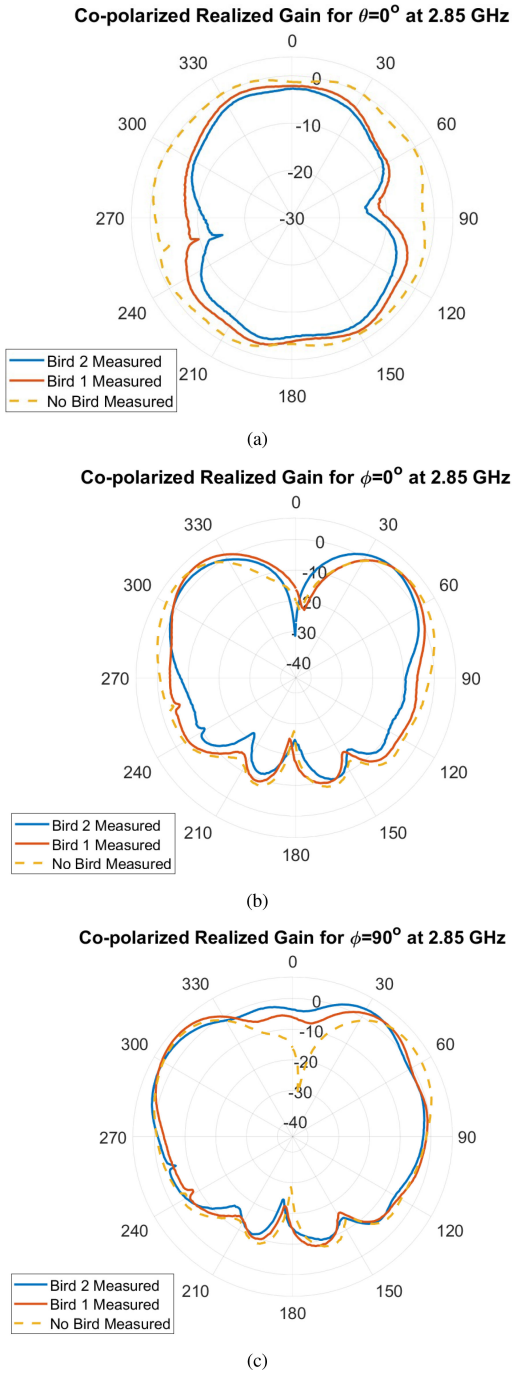


Fig. 5. Comparison of co-polarized radiation patterns of realized gain in dBi for the monopole measured with and without bird carcasses at 2.85 GHz for (a) azimuthal plane ($\theta = 0$), (b) elevation plane ($\phi = 0$), and (c) elevation plane ($\phi = 90°$) for the antenna and bird orientation shown in Fig. 3.

the radiation of the antenna than its impedance. In the azimuth cut plane there is a radiation dip around 270° from the feeding coaxial cable. In Fig. 5(c), a comparison of the copolarized elevation radiation pattern at $\Phi = 90°$ for the monopole antenna measured next to Bird 1, Bird 2, and free space. A noticeable impact of the presence of the birds on the radiation pattern of the monopole is that there is no longer a null at the top of the radiation pattern when the birds are present.

## IV. Bird Phantom Verification

Permittivity and conductivity values, given in Section II, for both ellipsoids of the phantom were found to match the measured and simulated results using parametric sweeps in HFSS. For comparison, a previously published saline model [7] was also simulated in HFSS as shown in Fig. 3(d); the shape of the outer volume in Fig. 1 was simulated without the inner ellipsoid, where the solid ellipsoid had properties of $\epsilon_r = 75$ and $\sigma = 2$ S/m. When used for experiments, this previous model consisted of a sponge filled with saline, which was carved in the shape of a bird. In Fig. 6, the magnitude of the insertion loss ($|S_{11}|$) and input impedance is shown for the bird phantom designed in this work (with the previously listed permittivity and conductivity values), the saline model, and the salvaged bird carcasses. This figure shows that the bird phantom published in this work presents a more accurate model than the saline model for impedance behavior.

In Fig. 7 the copolarized radiation patterns (at 2.85 GHz) are shown for the simulated bird phantom designed in this letter, the simulated results for the previously published saline model, and measured results for both of the salvaged bird carcasses. This figure shows that the phantom presented in this letter provides

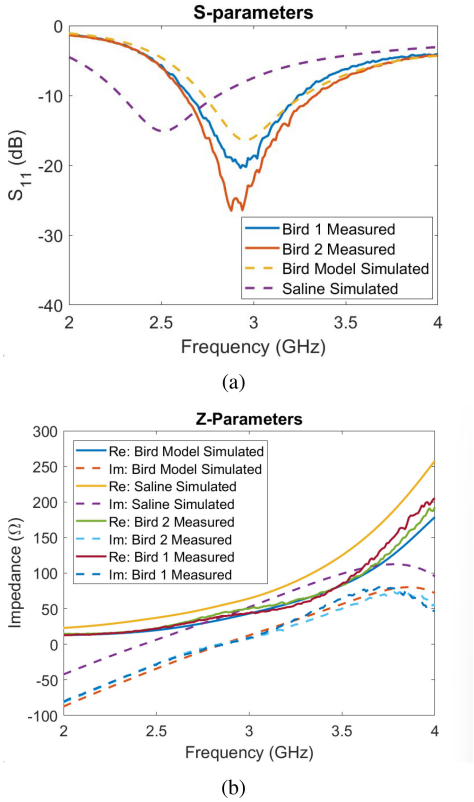


Fig. 6. Measurements of monopole with bird carcasses compared to simulations of monopole with the phantom shown in this work and the previously published saline model [7]: (a) Magnitude of insertion loss ($|S_{11}|$) in dB. (b) Input impedance ($Z_{11}$).

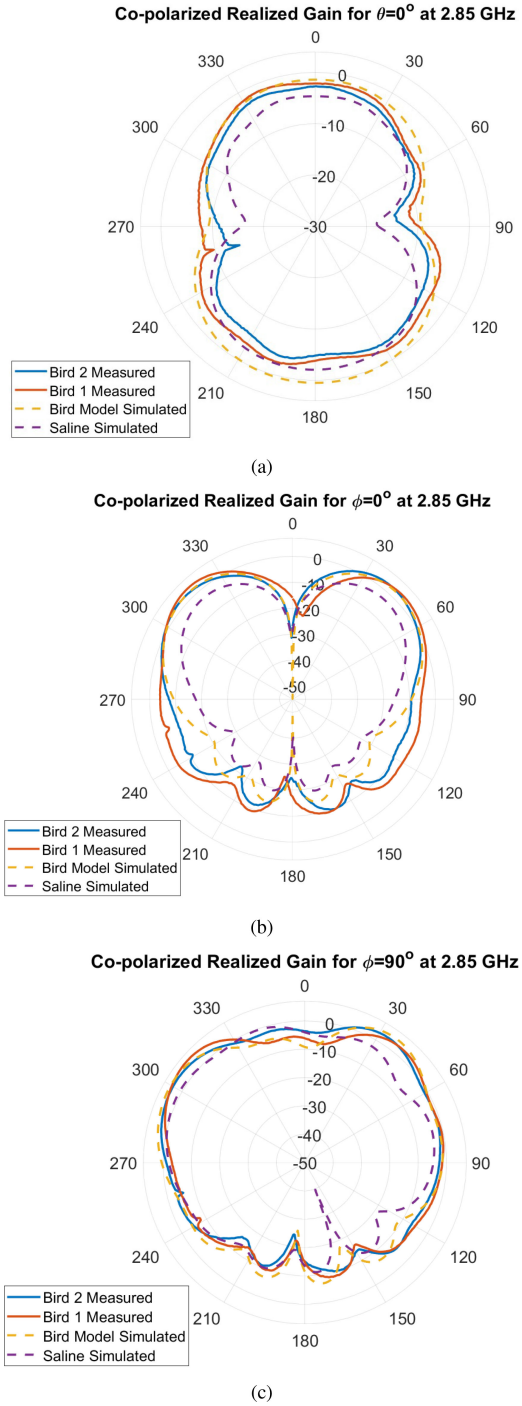


Fig. 7. Comparison of copolarized radiation patterns of realized gain in dBi for the monopole measured with bird carcasses versus the simulated monopole with the bird phantom shown in this work versus the previously published simple saline model [7] at 2.85 GHz for (a) azimuthal plane ($\theta = 0$), (b) elevation plane ($\phi = 0$), and (c) elevation plane ($\phi = 90^\circ$).

a better match with the measured results using bird carcasses than the previously published saline model for radiation. The saline model attenuates the radiation too extensively (indicating too much loss in the model).

In Fig. 7(b) and (c), the copolarized elevation radiation pattern is shown at $\phi = 0$ and $\phi = 90$, respectively. For the elevation radiation pattern at $\phi = 90$, it shows that the monopole simulated with the bird phantom presented in this letter does not have a null at the top of the radiation pattern—unlike the measured and simulated results of the monopole in free space. Comparing the results of the monopole with the simulated bird phantom and measured results for the monopole mounted with bird carcasses yields an RMS error of less than 7% for both return loss and the impedance less than 8% for realized gain.

## V. Conclusion

In conclusion, the electrical properties of our bird phantom model corresponded well with empirical measurements on salvaged carcasses of dark-eyed juncos. This phantom can be scaled for other bird species and will enable more effective bird tracking. The bird phantom is constructed of nested ellipsoids with $\epsilon_r = 1.2$ and $\sigma = 3$ S/m for the inner volume and $\epsilon_r = 1.2$ and $\sigma = 0$ S/m for the outer volume. This nested ellipsoid model was shown to be significantly more accurate than the only other previously published model, which equated bird body tissues to a uniform volume of saline. This work represents the first step toward a comprehensive phantom library to propel antenna designs for bird tracking technology. Future work should compare scaled versions of the phantom to different bird species and confirm model validity across a wider frequency range.

## REFERENCES


[1] E. S. Bridge *et al.*, "Technology on the move: Recent and forthcoming innovations for tracking migratory birds," *BioScience*, vol. 61, no. 9, pp. 689–698, 2011.

[2] E. S. Bridge and D. N. Bonter, "A low-cost radio frequency identification device for ornithological research," *J. Field Ornithol.*, vol. 82, no. 1, pp. 52–59, 2011.

[3] L. Hou, M. Verdirame, and K. C. Welch Jr., "Automated tracking of wild hummingbird mass and energetics over multiple time scales using radio frequency identification (RFID) technology," *J. Avian Biol.*, vol. 46, no. 1, pp. 1–8, 2015.

[4] W. Fiedler, "New technologies for monitoring bird migration and behaviour," *Ringing Migration*, vol. 24, no. 3, pp. 175–179, 2009.

[5] D. N. Bonter and E. S. Bridge, "Applications of radio frequency identification (RFID) in ornithological research: A review," *J. Field Ornithol.*, vol. 82, no. 1, pp. 1–10, 2011.

[6] E. S. Bridge *et al.*, "An Arduino-based RFID platform for animal research," *Front. Ecol. Evol.*, vol. 7, 2019, Art. no. 257.

[7] J. Martin, G. Swenson, and J. Bernhard, "Methodology for efficiency measurements of electrically small monopoles for animal tracking," *IEEE Antennas Propag. Mag.*, vol. 51, no. 2, pp. 39–47, Apr. 2009.

[8] ANSYS High Frequency Structure Simulator, "Ansys HFSS, 2018, " [Online]. Available: https://www.ansys.com/products/electronics/ansys-hfss

[9] V. Nolan Jr. *et al.*, "Dark-eyed junco *(Junco hyemalis)*," The Birds of North America Online. Ithaca, NY, USA: Cornell Lab of Ornithology, 2002.

[10] R. Kenward, *A Manual for Wildlife Radio Tagging* (Biological Techniques Series), rev. ed. San Diego, CA, USA: Academic, 2001. [Online]. Available: http://www.loc.gov/catdir/description/els031/00103147.html

[11] T. M. Pegan *et al.*, "Solar-powered radio tags reveal patterns of post-fledging site visitation in adult and juvenile tree swallows Tachycineta bicolor," *PLoS One*, vol. 13, no. 11, pp. 1–14, 2018. [Online]. Available: https://doi.org/10.1371/journal.pone.0206258

[12] J. H. Rappole and A. R. Tipton, "New harness design for attachment of radio transmitters to small passerines (nuevo diseño de arnés para atar transmisores a passeriformes pequeños)," *J. Field Ornithol.*, vol. 62, pp. 335–337, 1991.